Contents lists available at ScienceDirect

Process Safety and Environmental Protection

journal homepage: http://ees.elsevier.com

Improving of CI engine performance using three different types of biodiesel

K. Shojae [a], M. Mahdavian [b,*], B. Khoshandam [a], Hassan Karimi-Maleh [b,c,d]

[a] Faculty of Chemical Petroleum and Gas Engineering, Semnan University, Semnan, Iran
[b] Department of Chemical Engineering, Quchan University of Technology, Quchan, Iran
[c] School of Resources and Environment, University of Electronic Science and Technology of China, P.O. Box 611731, Xiyuan Ave, Chengdu, PR China
[d] Department of Chemical Sciences, University of Johannesburg, P.O. Box 17011, Doornfontein Campus, 2028, Johannesburg, South Africa

ARTICLE INFO

Article history:
Received 29 November 2020
Received in revised form 22 March 2021
Accepted 28 March 2021
Available online xxx

Keywords
Biodiesel
Fuel properties
Injection angle
Combustion chamber
Compression ratio

ABSTRACT

Currently, most automotive industries use fossil fuels, like diesel fuel, which are harmful for the environment and are known as the main reason for global warming. To reduce the adverse effects of these fuels, scholars have investigated and suggested green fuels like biodiesel. However, further studies should be conducted to improve the functionality of biodiesel fuel in diesel engines. In the current study, three completely distinct biodiesel fuels (namely, B1 with 96 % lauric oil, B2 with 88 % oleic oil, and B3 with 89.5 % ricinoleic oil) were numerically evaluated to carefully investigate the effects of the number of carbon atoms, the O—H bond, and viscosity on the performance of a CI engine. First, the predicted in-cylinder pressure, the rate of heat released, and NO emissions were compared to experimental results and an appropriate accord was obtained. For the mentioned biodiesels, the parameters of engine speed, injection angle, piston bowl center depth, and compression ratio were investigated by CFD code under different engine speeds. It was found that changing the piston bowl center depth (PBCD) value from 0.0042 to 0.009 m increased NO and the indicated power by 4% and 3%, respectively, for B1, B2, and B3 biofuels. In addition, when the engine was fueled by Corylus avellana biodiesel, the change in compression ratio from 16 to 24 increased peak pressure and torque by around 77 % and 17 %, respectively. The results showed that the cylinder fueled by high viscosity biodiesel has lower air-fuel mixing. A fuel that has more oxygen atoms in its chemical structure can produce higher NO emissions. Moreover, the injection angle of 150° led to increased fuel consumption rate and indicated power compared to the injection angle of 160°. It was determined that the compression ratio has significant effects on emission and combustion characteristics.

1. Introduction

Compression ignition (CI) engines are widely used by manufacturing companies of internal combustion engines due to their promising power performance. However, these engines commonly use diesel fuel and produce many pollutants such as nitrogen monoxide (NO), unburnt fuel, carbon dioxide (CO_2), carbon monoxide (CO), and soot. In recent years, many efforts have been made to develop clean fuels, especially biodiesel, which are known as promising fuels for CI engines because of their similar properties to diesel fuel. Biodiesels are renewably obtained from agricultural products and animal fats. It should be noted that the properties of these fuels, such as viscosity, number of carbon atoms, and the O—H bond, can highly affect the characteristics of the engine and should be carefully investigated (Ramadhas et al., 2005; Jiaqiang et al., 2016a). In addition, improving injection strategy, combustion chamber geometry, and EGR can enhance performance and reduce NO and soot emissions of a biodiesel-burning engine (Abu-Jrai et al., 2009).

Several studies have investigated the influences of fuel injection parameters like injection timing, injection pressure, etc. (Xu et al., 2016). Roy (2009) studied the fuel injection timing and pressure of a direct injection (DI) diesel engine. They showed that increasing the injection pressure or advancing the injection timing enhanced both peak cylinder pressure and mean in-cylinder temperature, simultaneously. Raeie et al. (2014) found that injection timing and pressure affect the performance and emissions of a diesel engine with a turbocharger. Fang et al. (2008) showed that the injection angle affects the emission and combustion characteristics of a high-speed direct-injection (HSDI) diesel engine. A reduction in NO emissions was seen for the narrow-angle injector because of better air-fuel mixing near the cylinder wall during the combustion process. The geometry of the combustion chamber has strong effects on the flow field. In addition, optimum air-fuel mixing within the cylinder cannot be created unless the injector–cylinder configurations are investigated in conjunction with each other (Yadollahi and Boroomand, 2013).

One technique for creating appropriate air-fuel mixture formation in the cylinder is modifying the combustion chamber configuration (Jiaqiang et al., 2016b), which can improve combustion and emission

* Corresponding author.
E-mail address: m.mahdavian@qiet.ac.ir (M. Mahdavian)

https://doi.org/10.1016/j.psep.2021.03.048
0957-5820/

characteristics (Choi et al., 2015). Importantly, the use of a modified combustion chamber can greatly reduce the emissions of a biodiesel fueled engine (Li et al., 2014). Lee et al. (2016) conducted experiments and numerical simulations to enhance the fuel efficiency of a diesel engine using a gasoline-diesel blended fuel. Numerical studies are done using KIVA−CHEMKIN multi-dimensional CFD code. Their results showed that suitable cylinder geometry enhanced fuel efficiency. Yaliwal et al. (2016) investigated the nozzle and combustion chamber geometry of a single-cylinder compression ignition engine operated with a methyl ester and producer gas induction. They achieved 5% increased brake thermal efficiency and reduced emissions. Kassaby and Allah (EL_Kassaby and Nemit_allah, 2013a) carried out studies on the compression ratio of a diesel engine and reported that its value changed in the range of 14 to 18. Results showed that NO emissions increased by 37 % when the compression ratio was changed from 14 to 18. Kakaee et al. (2016) conducted a numerical study on the piston bowl geometry of a RCCI dual-fuel engine. Their results determined that piston bowl depth can also affect emissions from engines, especially UHC and CO emissions.

Buyukkaya (2010) examined neat rapeseed oil in a diesel engine and its blends of 5%, 20 %, and 70 % with diesel fuel under various engine speeds. They showed that soot emissions can be dramatically reduced by using pure biodiesel compared to diesel. Gupta and Dubey (Dubey and Gupta, 2017) conducted an experimental investigation on a naturally aspirated diesel engine fueled by dual biodiesel blends and showed that NOx, HC, CO and soot emissions would be significantly reduced by this combined fuel. Ibrahim (2016) investigated blends of butanol–biodiesel–diesel and showed that NO emissions were increased when the oxygenated oil was increased in the fuel compound. Yang et al. (2016) showed that brake specific fuel consumption was increased by using a proportion of isobutanol in biodiesel-diesel blended fuel. E et al. (Jiaqiang et al., 2016a) examined FAMEs in a diesel engine (under 2400 rpm engine speed). They indicated that soybean and rapeseed biodiesels produced lower NO and engine power, because they have some high viscosity oils in their fuel compound.

The literature showed that many scholars have investigated various compression ignition engines fueled by biodiesels with only relative differences in structural and chemical properties, and the feedbacks of these biodiesels were compared with each other. When biodiesels with high differences in properties are not chosen, in cases of viscosity, the number of carbon atoms, and the O—H bond, the previous results can be affected by other properties of the fuel. In addition, for a case study, the influence of engine speed, injection angle, piston bowl center depth and compression ratio on the aforementioned biodiesel properties is not determined simultaneously (Jiaqiang et al., 2016a). These issues are addressed in the present study. In the present paper, three biodiesel fuels (see Table 3) with distinct properties in terms of viscosity, the number of carbon atoms, and the number of O—H bonds were selected to study the direct effects of these properties on engine performance. From the selected biodiesels, B1 (rich lauric oil) has 6 carbon atoms less than B2 (rich oleic oil), and B3 (rich ricinoleic oil) and B3 have an O—H bond. In addition, B1, B2, and B3 have different viscosities. Therefore, based on the selected biodiesels, investigating the effects of the number of carbon atoms, O—H bond, and viscosity values on emissions and engine performance can be performed more accurately than in previous studies (Jiaqiang et al., 2016a; Mobasheri and Peng, 2013). Moreover, two important parameters of the combustion chamber (injection angle and piston bowl geometry) were selected and modified to enhance engine performance when using B1, B2, and B3, which has not been considered in previous research (Jiaqiang et al., 2016a).

The present study consists of three sections. First, the grid is created according to a direct injection (DI) Toyota engine. Then, in-cylinder mean pressure, rate of heat released, and NO emissions are validated by experimental data. Finally, emission and combustion parameters of biodiesels with different properties under various engine speeds are calculated. Moreover, the effects of piston bowl center depth, compression ratio, and injection angle on the performance of the engine have been calculated. This can help overcome lower fuel-air mixing caused by the high viscosity of some oils in fuel compounds or enhance combustion performance of low calorific value biodiesels used in the engine.

2. Simulation

2.1. Methodology

The numerical simulation in the present work was performed using AVL Fire code software. The load is maintained by constant fuel mass injection. This code is now being used and validated for the simulation of various combustion processes (Mobasheri and Peng, 2013). Here, 3-deminsonal (3D) and 2-deminsonal (2D) simulations were performed by the mentioned software. Most of the results are in 3D and 2D, simultaneously. Table 1 denotes the models applied for simulation. To predict turbulence, the k-zeta-f model was used. This turbulence model solves a transport equation for the velocity scales ratio as:

$$zeta = \frac{\vartheta^2}{k} \tag{1}$$

where ϑ^2 is velocity scale and k is the turbulence kinetic energy. The k-zeta-f model is useful in the gas nozzle area, where wall effects are inevitable (Kapusta and Teodorczyk, 2012). The ECFM combustion model relies on a flame surface density transport relation, which can define diffusion combustion and inhomogeneous turbulent premixed flames. This model calculates the mean fuel reaction rate for turbulent combustion by a 2-step chemistry mechanism, as follows (Mobasheri and Peng, 2012):

$$C_aH_bO_c + \left[a + \frac{b}{4} - \frac{c}{2}\right] O_2 \rightarrow a\,CO_2 + \frac{b}{2}H_2O \tag{2}$$

$$C_aH_bO_c + \left[\frac{b}{2} - \frac{c}{2}\right] O_2 \rightarrow a\,CO + \frac{b}{2}H_2 \tag{3}$$

where a, b and c are the number of carbon, hydrogen and oxygen.

The ECFM-3Z combustion model was used for ignition modelling. This model explains the fuel consumption amount per unit volume by the product of the flame surface density. The growth of an initial turbulence on a liquid face considering this model is related to its wavelength and other physical parameters (Manual, A.A.F.U. and C. Fire, Solver, 2013).

The Dukowicz model was employed to evaporate droplets. This model is based on the comparison of heat and mass transfer near the droplet surface. In this model, the vicinity of the droplet flow is spherically symmetrical. There is a quasi-stationary layer of liquid vapor in the vicinity of the droplet surface. Thermodynamic equilibrium between vapor and liquid on the surface of the droplets is considered. The gas properties are constant near the droplets, and uniformity of droplet temperature is confirmed (Semenov et al., 2013). From various break-up models, the wave model was chosen. This model specifies how droplets separate by predicting the wavelength of the fastest growing disorders on a liquid droplet surface because of aerodynamic variations (Pizza et al., 2007). In the diesel engine due to the high operat-

Table 1
Models applied for whole simulations of the present work.

Parameter	Predicted by
Turbulence	k-zeta-f
combustion	ECFM
Evaporation (spray)	Dukowicz
Break up (spray)	Wave
NO emission	Extended Zeldovich
Soot emission	Kinetic model

ing temperature, the fuel and prompt NO, emissions are negligible. To predict thermal NO, the extended Zeldovich can be used. Based on this model, three principal reactions that produce thermal NO emissions are as follows (Mobasheri and Peng, 2012):

$$\begin{aligned} N_2 + O &\leftrightarrow NO + N \\ N + O2 &\leftrightarrow NO + O \\ N + OH &\leftrightarrow NO + H \end{aligned} \quad (4)$$

Soot formation was modeled using the kinetic model. It suggests an accurate chemical reaction scheme to predict both soot formation and oxidation. The kinetic model considers the mechanisms of formation of hydrocarbons, polyynes, etc., and based on this model, the local equivalence ratio changes the soot formation reaction parameters, and the soot is oxidized because of the presence of O_2 and H_2O (Mobasheri and Peng, 2012). Tables 2 and 3, show the biodiesel compositions considered in this work. B0 fuel was only selected for validation and mesh sensitivity analysis sections, and B1, B2, and B3 are considered as simulation assays.

Shahbazi et al. (2012) Changed the composition and some physical properties of RBD palm oil by using NaOH as a catalyst. They showed that the biodiesel synthesized by this catalyst had proper properties compared to diesel fuel. In the present paper, three biodiesel fuels were selected based on the composition of the synthesized biodiesel (B0) as follows: B1 was chosen because of its high lauric oil content (96 %), which has lower viscosity and calorific value compared to B2 and B3; B2 was selected for its higher oleic oil (88 %) and has lower viscosity than B3; B3 was chosen because of its high ricinoleic oil (89 %), and it has a stronger O—H bond in its chemical structure and high viscosity and calorific value compared to oleic and lauric oils (Singh and Singh, 2010).

In this paper, a light-duty 2KD-FTV Toyota engine was chosen and modeled. The engine specifications are presented in Table 4. Simulations of the engine started at IVC (-150 °CA) and ended at EVO (+90 °CA) in a closed cycle.

The piston scheme is presented in Fig. 1. The boundary conditions were applied as follows: piston 555 K (wall-mesh movement), liner (wall) 430 K, and head (wall) 520 K. The simulation conditions of each considered fuel are presented in Table 5.

Table 2
Pure biodiesel compositions (B0) considered for validation and mesh sensitivity analyze sections (Cm: n, oil composition, percentage by weight).

Type	B0 (Jiaqiang et al., 2016a)
Methyl palmitate (C16:0)	10.13
Methyl oleate (C18:1)	53.4
Methyl stearate (C18:0)	8.34
Methyl linoleate (C18:2)	2.38
Methyl eicosenoate (C18:3)	7.63
Methyl docosanoate (C22:0)	1.58
Methyl tetracosanoate (C24:0)	1.38

Table 3
Compositions and viscosity of biodiesels considered to simulation assays.

Oil type	Viscosity (m/s^2) at 40 °C (Li et al., 2017; Yang et al., 2015a)	B00 (Singh and Singh, 2010)	Corylus Avellana (CA) (B2) (Özgür and Tosun, 2017)	Castor (B3) (Li et al., 2017)	Litsea Glutinosa Robins (LGR) (B1) (Özgür and Tosun, 2017)
Myristic (C14:0)	3.46	1.14	3.2	0	0
Lauric (C12:0)	2.5	0	0	0	96.3
Palmitic (C16:0)	4.4	42.04	3.1	1.6	0
Palmitoleic (C16:1)	3.6	0.14	0	0	0
Stearic (C18:0)	5.1	4.43	2.6	0.9	0
Oleic (C18:1)	4.6	39.97	88	3	2.3
Linoleic (C18:2)	3.7	11.74	2.9	3.7	0
Linolenic (C18:3)	3.2	0.44	0	0.4	0
Ricinoleic (C18:1-OH)	14.3	0	0	89.5	0
Arachidic (C20:0)	6.7	0.09	0	0.3	0
Behenic (C22:0)	–	0	0	0.6	0

Table 4
Engine specifications (Jiaqiang et al., 2016a).

Type	Light-duty 2KD-FTV Toyota engine
Bore	92 m
Stroke	93.8 m
Swept volume	2.494 L
Connecting rod	158.5m
Compression ratio	18.5
Fuel injection holes	6
Nozzle radius	45 nm

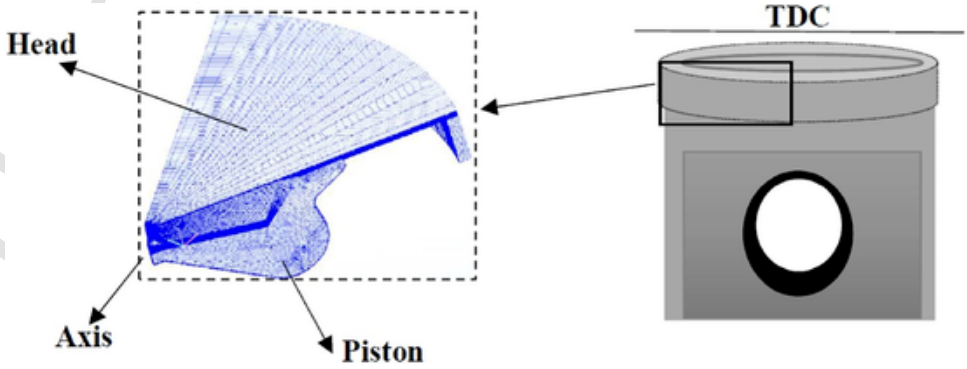

Fig. 1. Piston scheme and designed grid of a part of piston bowl at TDC position.

Table 5
Simulation parameters considered for various fuels (Jiaqiang et al., 2016a; Yang et al., 2015b).

Parameters	Diesel	B0	Other oils
Initial pressure (bar)	1.875	1.87	1.87
Initial temperature (K)	350	350	350
Injection timing (ºCA)	−14	−10	−10
Injection temperature (K)	330	330	330
Engine speed (rpm)	Variable	2400	Variable

2.1.1. Mesh sensitivity analyses

The calculated mean pressure of the cylinder is presented in Fig. 2 for the different numbers of meshes from 40,000 and more for the engine fueled by B0 under 2400 rpm engine speed and full load conditions. It was observed that the curves were identical with each other after 70,000 meshes, so this number of meshes is considered sufficient.

2.1.2. Validation

To validate the model, the calculated results were compared with the experimental data for mean pressure, rate of heat released, and NO emission for the neat diesel and B0 fuels at no EGR conditions. The conditions considered for validation are presented in Table 5 (B0 and diesel). Fig. 3 shows the comparison between experimental and calculated mean pressures of cylinder, rates of heat released, and exhaust NO (Jiaqiang et al., 2016a; Özgür and Tosun, 2017; Li et al., 2017; Yang et al., 2015a). As seen, the calculated results of pure diesel and biodiesel are in good agreement with the experimental data, but there is only a general accord between the experimental and calculated rate of heat released data.

Generated errors for the rate of heat released can occur when calculations do not consider thermal radiation, latent heat of vaporization, etc. As shown in Fig. 3, the predicted exhaust NO was below experimental values, possibly due to neglecting fuel and prompt NO in the extended Zeldovich reaction mechanism and the thermal radiation and other heat transfers, which can change the in-cylinder temperature. Furthermore, choosing other models like soot and fuel reaction mechanisms can affect the oxygen content and conversation of N to NO. However, these errors exist in similar works and are common in engine simulations (Jiaqiang et al., 2016a; Yang et al., 2015b; Li et al., 2016). Because the simulation was validated for pure diesel and biodiesel, changing fuel compounds and simulating the engine with other biodiesels in the pure state are reasonable. To further ensure accuracy, comparisons between fuels under the same conditions should be done.

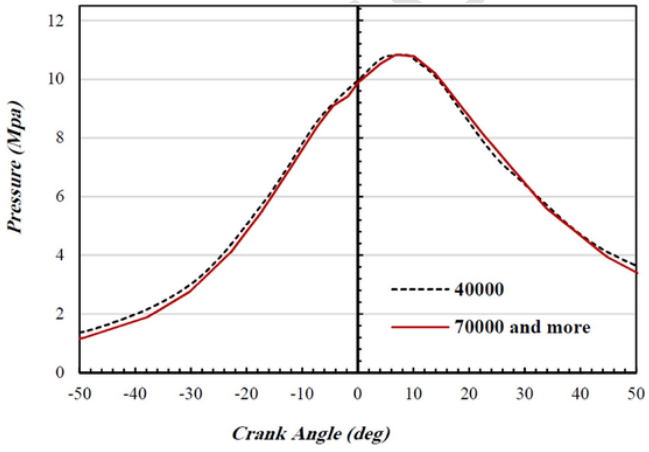

Fig. 2. Grid independence analyze for the range of meshes from 40,000 and more.

3. Results and discussion

In this section, the effects of engine speed, injection angle, piston bowl center depth, and compression ratio of the engine fueled by pure biodiesels on indicated power, thermal efficiency, brake specific fuel consumption (BSFC), CO, CO2, HC, NOx, and soot emissions are determined and discussed. Furthermore, the equivalence ratio distribution of pure diesel is compared to those of B2 and B3. The variation of spray angle can have high effect on air-fuel mixing conduct in the cylinder. By changing the spray angle, the required time for the collision of fuel on piston bowl wall is changed, which can highly affect the time of creating the vortexes. Hence, we considered different injection angle to investigate different functional behavior of this parameter. For increasing the air-fuel mixing and the performance of a diesel engine, the combustion chamber geometry is known a very important parameter. Changing the bowl center depth can affect the velocity direction of air that has significant effects on air-fuel mixing. In Fig. 13, more air flow turbulence for Tm3 is obvious due to increasing the piston bowl center depth. Engine speed is an effective and well-known parameter in engine research. However, we considered this parameter for examining its effects on our case study, diesel engine fuelled by different biodiesels, for investigating the performance outcomes from using three biodiesels with high differences in chemical structure.

3.1. Comparison of biofuels at different engine speeds with a base engine configuration

Fig. 4 denotes variations in exhaust NO and soot generated by the engine considering different biodiesel compounds on engine speed. The lowest exhaust NO was determined to be the B1 fuel under engine speeds of 1500 rpm and 2500 rpm. Higher NO emissions of B3 under 1500 and 2500 rpm engine speeds were due to the higher oxygen content and calorific value of ricinoleic oil that consists of 89 % B3 fuel, and this leads to increased NO emissions (Ibrahim, 2016). Under high engine speeds, there is not enough time to perform chemical reactions and the heat transfer completely, both of which can highly impact the temperature of the cylinder (i.e. less time for chemical reactions leads to lower temperature, but reducing the heat transfer results in higher temperature). Generally, the combination effect of the mentioned parameters resulted in lower NO emissions and more soot emissions due to the reduction in the in-cylinder temperature. As seen in Fig. 4, there are almost no difference between NO emissions for B1, B2 and B3 at 3500 and 4500 rpm engine speed. It is demonstrated that at high engine speed, in-cylinder temperature is not enough to provide a complete reaction for B3 and its NO emission is equal to B1. In high engine speeds the in-cylinder temperature reduces and a high viscosity fuel like B3 has not enough air-fuel mixing, which led to increasing soot emissions due to lower soot oxidation. Therefore, engine speed has dominant effect on the in-cylinder NO emissions compared to dramatic differences in fuel chemical structure.

Nevertheless, ricinoleic oil has a higher viscosity value compared to lauric and oleic oils that consist of 96 % and 88 % of B1 and B2 fuels, respectively, which may lead to a reduction in the NO emissions of B3 due to lower air-fuel mixing. However, the higher calorific value and oxygen content of B3 are dominant parameters and can explain the higher NO emissions of B3 compared to B1 and B2. It was observed that B2 produced more exhaust NO compared to B1 and B3 under 3500 and 4500 rpm engine speeds. In order to find it reasonable, the in-cylinder temperature and oxygen distribution at various crank angles are presented in Fig. 5 for the 3500 rpm engine speed. As seen, under this engine speed, B2 produced a wide high-temperature zone ranging from 10 to 90 ˚CAs, which led to more oxygen consumption. Thus, considering this high-temperature area and the higher NO emissions for B2 in comparison with B1 and B3, it can be concluded that NO is mostly dependent on high-temperature areas, and nitrogen can increasingly react with oxygen in these zones; therefore, the higher exhaust NO in this

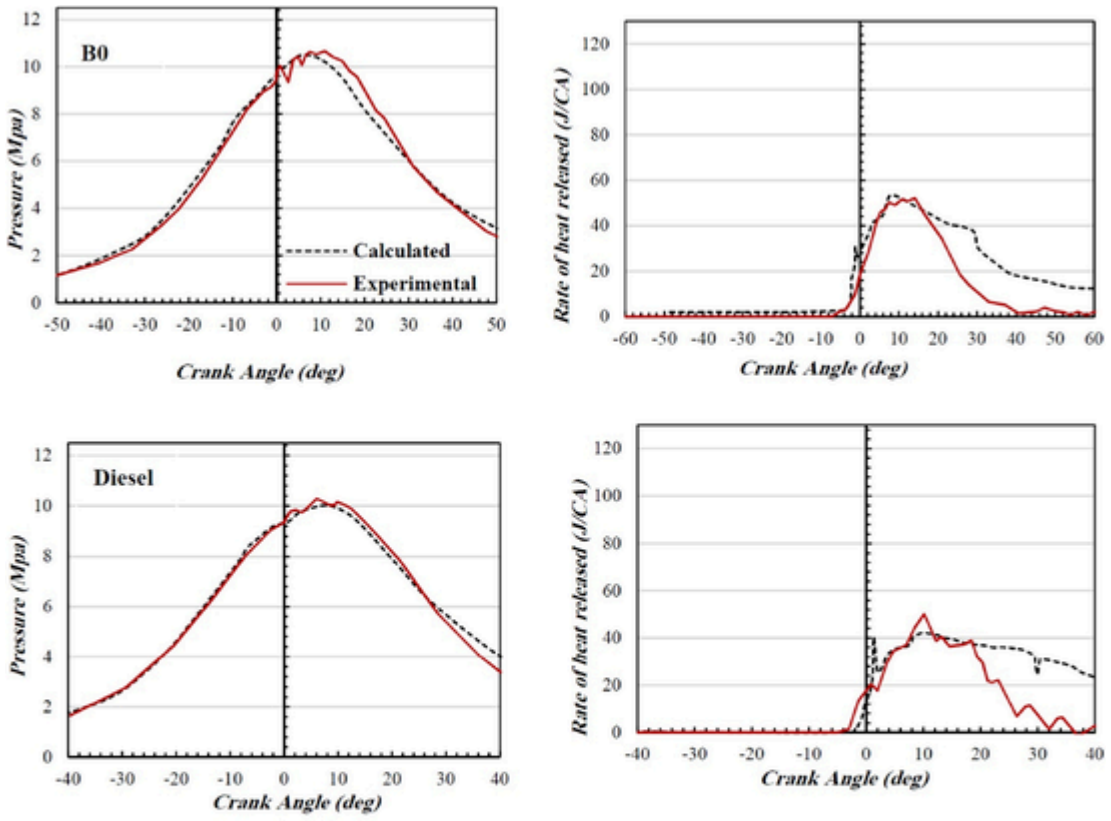

Fuel type	NO (predicted)	NO (experimental)
Diesel (gram)	3.1 e-5	4.8 e-5
B0 (ppm/kW)	11.14	14.42

Fig. 3. Comparison of calculated and experimental results (Jiaqiang et al., 2016a; Yang et al., 2015b; Li et al., 2016) for pure diesel and B0 fuels.

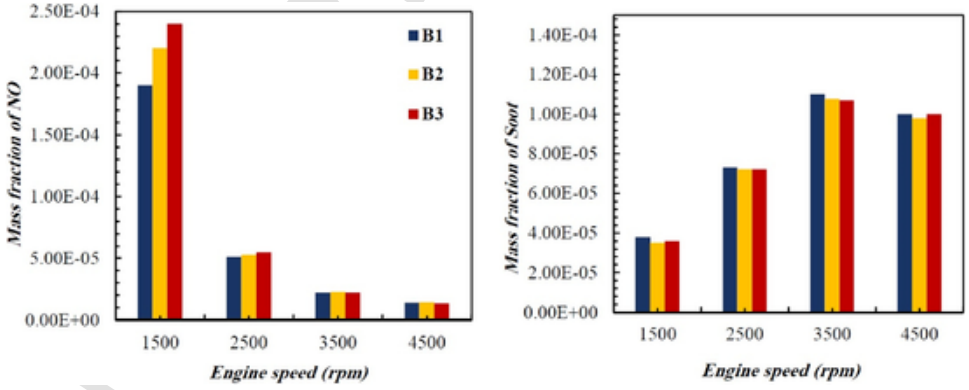

Fig. 4. Amount of exhaust soot and NO under different engine speeds of 1500, 2500, 3500 and 4500.

engine speed is due to this wide high-temperature area, which may be caused by the fuel's lower viscosity compared to B3 and higher calorific value compared to B1. Moreover, B1 produced higher soot emissions in different engine speeds, because it made lower peak pressure (as shown in Fig. 6) due to its lower calorific value, which means a lower temperature and reduced soot oxidation, and this explains the higher exhaust soot emissions from the engine fueled by B1.

As seen in Fig. 4, NO emissions were reduced by increasing engine speed, while soot increased up to the engine speed of 3500 rpm. This is due to the reduction in peak pressure at higher engine speeds, which led to a reduction in the in-cylinder temperature and subsequently lower soot oxidation and NO emissions. The effects of engine speed on the indicated power, thermal efficiency, peak pressure, and BSFC histories for B1, B2, and B3 are depicted in Fig. 6. As determined, increases in engine speed enhanced engine power (up to 3500 rpm), but reduced indicated thermal efficiency. Under the same conditions, higher engine speed can delay combustion timing, so the accessible time for chemical reactions is decreased, which results in lower peak pressure and higher

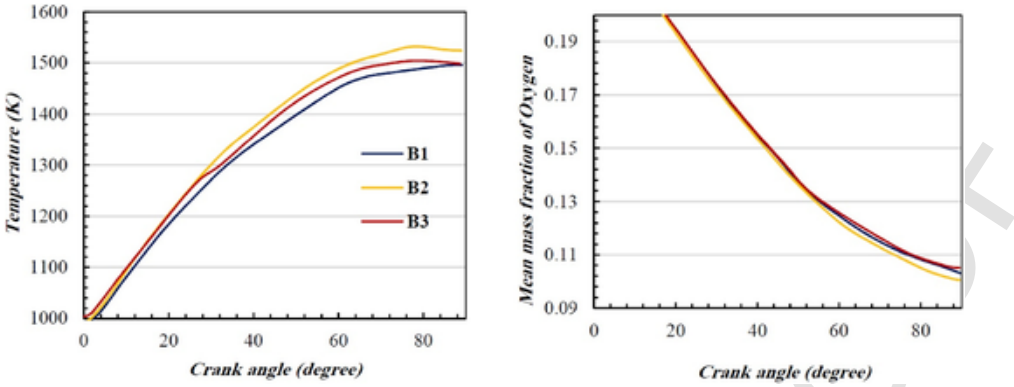

Fig. 5. Temperature and oxygen distribution versus crank angle for different fuels under 3500 rpm engine speed.

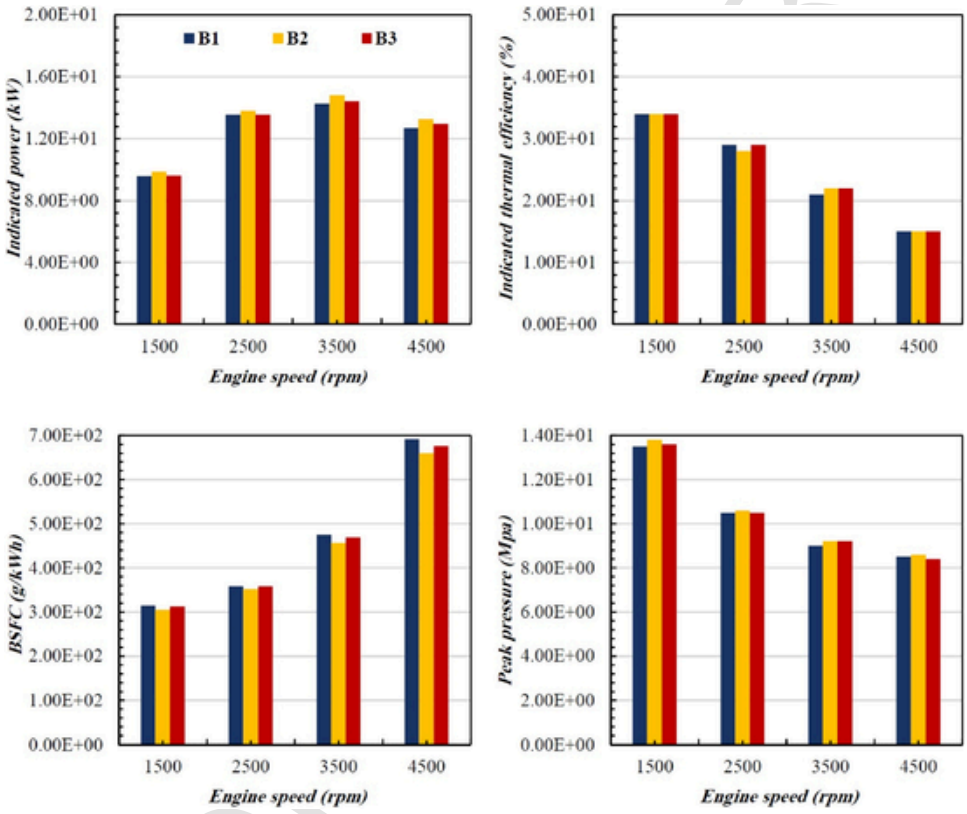

Fig. 6. Comparison of BSFC, indicated thermal efficiency, indicated power, and peak pressure between B1, B2, and B3 fuels.

incomplete combustion (Kakaee et al., 2015). As illustrated, the three considered fuels had the same thermal efficiency rates under 1500 rpm engine speed, but this parameter changed at engine speeds of 2500 and 3500 rpm, yet became identical again under the engine speed of 4500 rpm. As previously mentioned, higher NO emissions can also be caused by the B3 fuel having more oxygen in its chemical structure; this fuel is a more oxygenated fuel compared with B1 and B2. These effects have been also observed in reference Ibrahim (2016).

The BSFC parameter determines fuel efficiency. As seen, B1 had higher BSFC under engine speeds varying from 1500 rpm to 4500 rpm. Therefore, more B1 should be consumed to meet a constant power in comparison with the other fuels. In Fig. 7, the variations of burnt fuel mass fraction at various crank angles are presented for B1, B2, and B3. B1 has lower viscosity compared with B3 and B2, resulting in better air-fuel mixing; this can be a major reason for more B1 consumption under the engine speed of 4500 rpm. It should be noted that almost the same results were obtained for other engine speeds, but only the results at 4500 rpm are presented. In Fig. 6, it can be observed that B1 created lower peak pressure and indicated power because of its lower CV compared to B2 and B3.

The equivalence ratio distribution for B1, B2, and B3 fuels at various crank angles is shown in Fig. 8. As can be seen, B1 has a smaller equivalence ratio compared with B2 because of the fact that it has the most lauric oil, which leads to better air-fuel mixing and more complete combustion (lauric oil has low viscosity). However, B1 created lower peak pressure and power in most engine speeds (as shown in Fig. 6), despite having better air-fuel mixing, which can be explained by its lower CV. Thus, for B1 fuel or a blend of it with diesel fuel, air-fuel mixing should be further improved by modifying the combustion chamber geometry, injection angle, etc., to further reduce unburned fuels and fuel costs. B3 also had a lower equivalence ratio compared to B2, which can be explained by the higher oxygen content of ricinoleic oil (B3 includes the largest amount of ricinoleic oil by 96 %), which leads to a reduced mean equivalence ratio (Chen et al., 2014). For

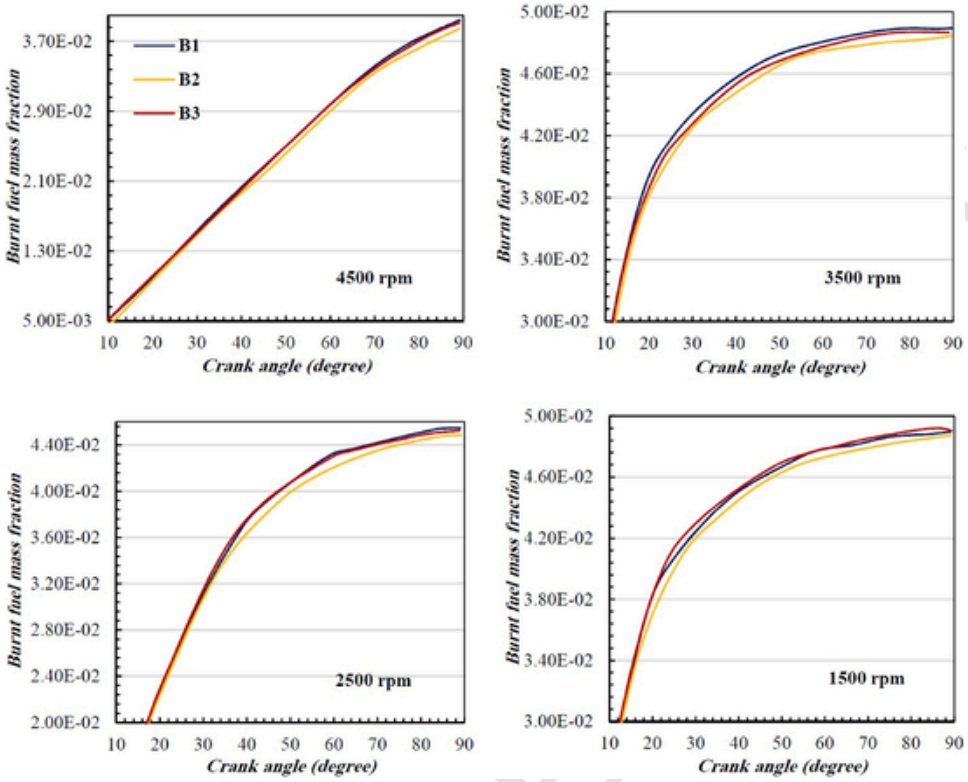

Fig. 7. Burnt fuel mass fraction versus crank angle for different biodiesels under various engine speeds.

B3, the reason for the greater burnt fuel mass fraction and higher NO emissions compared to B1 is its lower cetane numbers, which led to increased NO emissions (Fig. 7). In addition, due to the decrease in ignition delay, the lower cetane number of B3 can decrease the size of the premixed combustion. It can lead to lower rates of NO formation, because the in-cylinder pressure slowly increases, and localized gas temperatures diminish through heat transfer and dilution (Kalligeros et al., 2003).

Hydrocarbon (HC) emissions in a diesel engine are composited of unburned fuels as a result of inadequate in-cylinder temperature, which forms near the combustion chamber wall. For this reason, the temperature of the air-fuel mixture is significantly lower than the center of the combustion chamber. In diesel engines, engine speed, engine load, combustion chamber design, etc. affect the number of hydrocarbon emissions (Reşitoğlu et al., 2015). Fig. 9 shows a comparison of HC, CO, and CO_2 emissions for fuels B1, B2, and B3 under various engine speeds. As can be seen, HC, CO, and CO_2 emissions of an engine fueled by B1 are lower than those of other fuels due to its better air-fuel mixing, more complete combustion, and fewer carbon atoms in its chemical structure under the same conditions and engine speeds lower than 4500 rpm. As seen in Fig. 9, the HC emissions of B1 is lower than B3 at 1500 rpm engine speed but under high engine speed (4500 rpm) it is higher than B3. In addition, B2 produced higher HC compared to B1 and B3 at considered engine speeds. Particularly, at high engine speeds, where the in-cylinder temperature is dramatically reduced, even B1 with 12 carbon atoms has not a completer combustion compared to B3 with 18 carbon atoms. Lower CH emissions from the engine fueled by B3 compared to B1 at 4500 rpm engine speed is the existed O—H band in its chemical structure, which led to more CH oxidation.

3.2. Injection angle

In this section, combustion parameters and emission results for a CI engine fueled by B1, B2, and B3 under a speed of 2500 rpm are presented for different injection angles. The effects of injection angle are analyzed to find a proper injection angle that can improve air-fuel mixing, combustion and emission characteristics. Fig. 10 shows a scheme of fuel distribution at various injection angles. As can be seen, at the injection angle of 150°, injected fuel strikes the piston bowl wall and spreads in the cylinder faster than at the 160° injection angle, so it is expected that the 150° injection angle can improve fuel consumption compared to 160° due to its better air-fuel mixing. Fig. 11 illustrates the burnt fuel mass fractions and temperature distributions for different biodiesels under injection angles of 140°, 150°, and 160°. It was found that the burnt fuel mass fraction and the in-cylinder mean temperature were higher for the injection angle of 150° than other spray angles for the considered fuels due to improved air-fuel mixing, as previously predicted.

As seen in Fig. 11, for all considered fuels, changing the spray angle from 160° to 140° led to reducing the mean pressure and burnt fuel mass fraction since fuel injected at 140° spray angle accumulated on bottom of the piston bowl more than other spray angles (as denoted in Fig. 10) and lack of proper spreading fuel within the cylinder had negative effects on air-fuel mixing and lower in-cylinder temperature is due to lower air-fuel mixing and complete combustion. Moreover, it is determined that changing the spray angle did not affect the air-fuel mixing before the TDC point and reducing the spray angle from 160° to 150° has not changed the ignition delay. It can be justified by the fact that after fuel injection (about 10 CA BTDC) a short time is needed to strike fuel with piston bowl wall and creating more turbulences so changing spray angle effects on air-fuel mixing are only seen after TDC point and did not change ignition delay duration.

To better comprehend the effects of improved air-fuel mixing, the in-cylinder mean pressure and accumulated heat release concerning the crank angles for three biodiesels and three injection angles under a constant engine speed are presented in Fig. 12.

In the process of reducing NOx emissions, operating conditions like reaction temperature and residence time are very determinative. For the injection angle of 160°, the later collision of fuel with the bowl wall and less fuel retention near the piston bowl wall led to better air-fuel

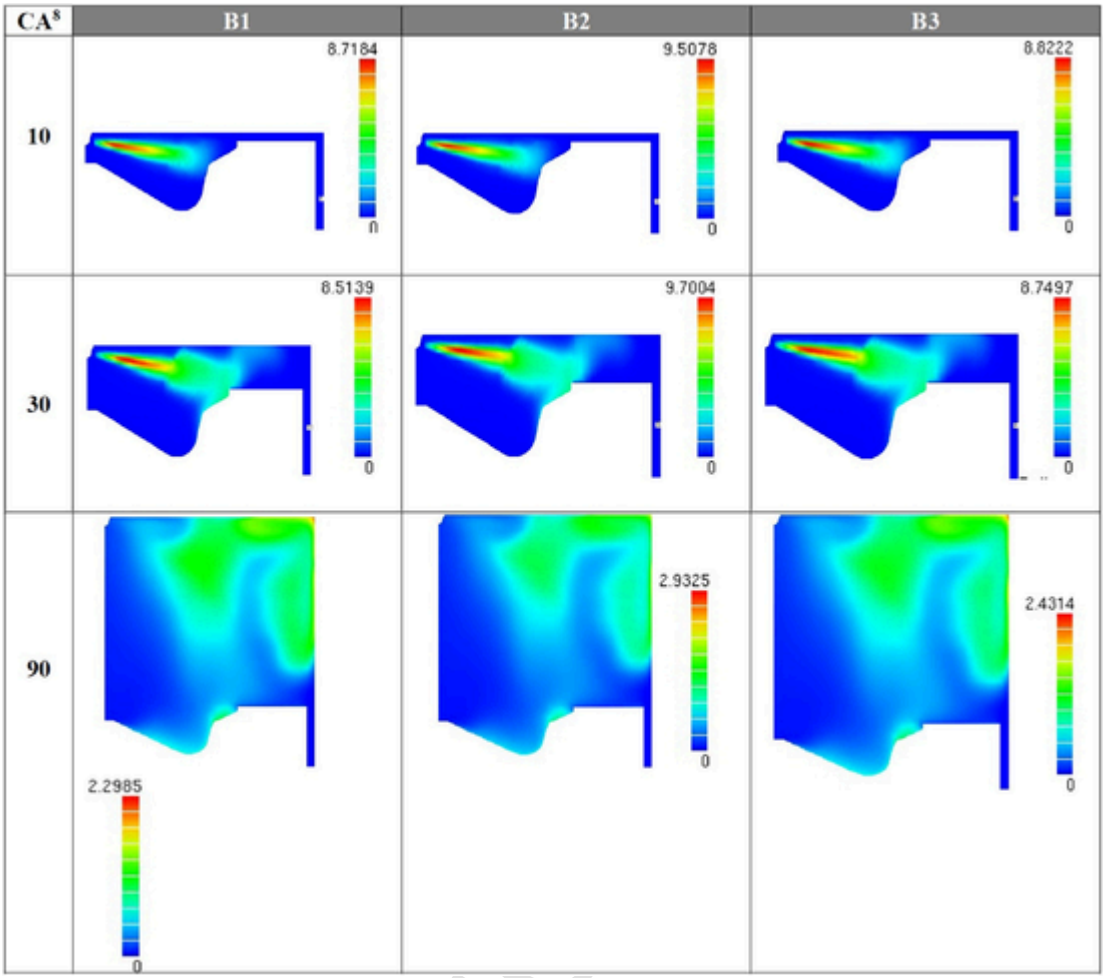

Fig. 8. Comparison of in-cylinder equivalence ratio distribution at 10, 30, and 90 CAs ATDC for B1, B2, and B3 under 3500 rpm engine speed.

mixing and fuel consumption, resulting in a higher temperature of combustion (refer to Fig. 10). The mean pressure and accumulated heat release were different for B1, B2, and B3 at various injection angles, and the injection angle of 150° increased the mean pressure and accumulated heat release compared to the 160° and 140° angles. Thus, to enhance the air-fuel mixing of high-viscosity biodiesels, the 150° injection angle is suggested for the engine. It is further expected that this injection angle will also be preferable in the case of air-fuel mixing for other fuels, like a blend of biodiesel and diesel for the engine introduced in this paper (150° spray angle led to more peak pressure and accumulated heat release in all engine speeds, but only the results at 2500 rpm are presented). The higher in-cylinder pressure and temperature zone of B2 compared with B1 and B3 is because of its lower ignition delay. B2 is ignited faster and more fuel is consumed compared with B1 and B2.Therefore, the engine fueled by B2 had a higher pressure zone and earlier pressure rise than B3 and B1. As seen in Fig. 14, the RHR for B3 was lower than that of B2 and B1, due to the higher kinetic viscosity of B3 which causes poor spray, evaporation, and air-fuel mixing process in the cylinder (Jiaqiang et al., 2016b).

3.3. Combustion chamber

Modification of the combustion chamber geometry can improve combustion performance and reduce emissions. A cylinder geometry which enhances TKE and swirl intensification will cause more efficient combustion. To apply an appropriate swirl and TKE in the cylinder at the time of ignition to enhance the combustion performance, choosing a combustion chamber that generates swirl is preferable. It has been shown that piston bowl geometry can induce swirl and TKE intensification around TDC (Reddy et al., 2015; Woo and Kim, 2019). Piston bowl center depth and compression ratio have dramatic effects on flow motion and turbulences. Therefore, the effects of bowl center depth and compression ratio on TKE and swirl have been investigated, because these parameters can increase air motion before fuel ignition and consequently affect mixing processes. The bowl center depth parameter is introduced in Fig. 13.

Because of enhancing the area to volume ratio, the heat losses are increased by increasing piston bowl depth, resulting in improved combustion efficiency, indicated power and negative effects like increasing NO emissions (Choi et al., 2015). In addition, the air direction and velocity within cylinder equipped with three different bowl center depth (BCD) lengths of 0.0042, 0.007, and 0.009 m, are different for each other and Tm2 and Tm3 created strongly convolute air flows with higher airspeed than Tm1, which have beneficial effects on air-fuel mixing and ignition delay. The effects of changing BCD on swirl and TKE for B1, B2, and B3 under different engine speeds are investigated but only results of B1, B2, and B3 at 2500 rpm engine speed are presented in Fig. 14 because analyzes of these fuels almost gave the same results at different engine speeds in the case of swirl ratio and TKE changes.

Significant differences were observed between the swirl ratios of Tm1, Tm2, and Tm3. In fact, towards the TDC point, the differences in swirl and TKE of all the geometries were considerable; a different trend was seen the TKE distribution. It was found that the flow field at the end of suction (near the TDC) is dependent upon the piston bowl center depth design. As can be seen in Fig. 14, by increasing the BDC from

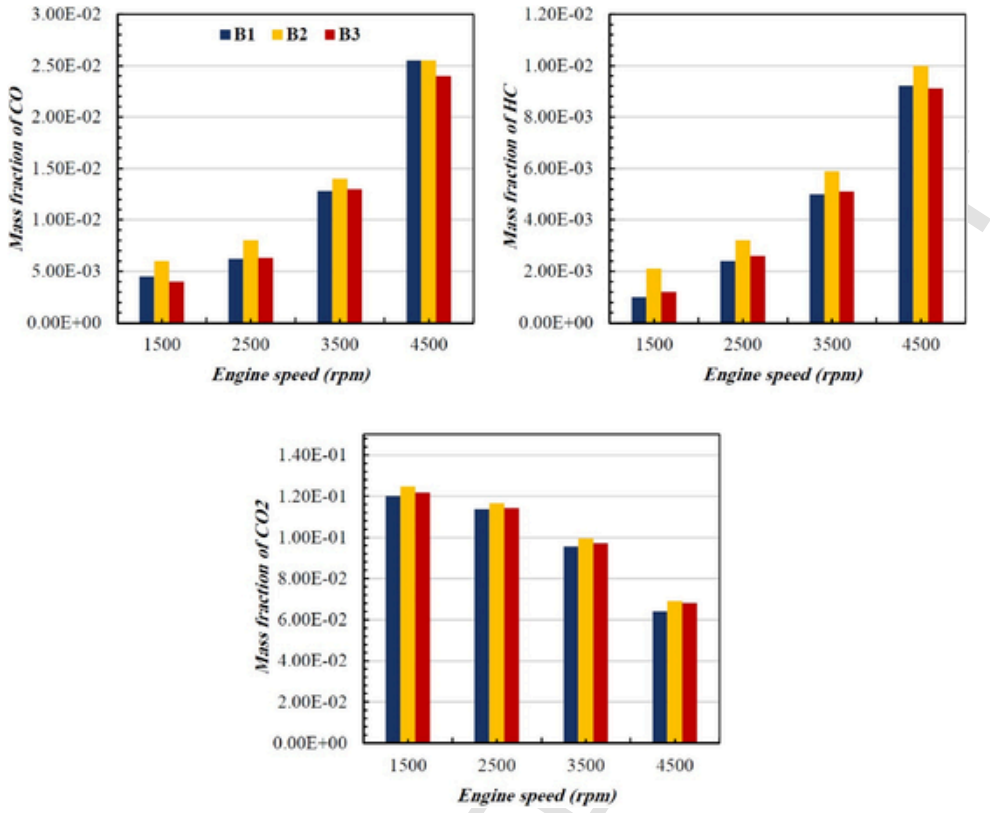

Fig. 9. Amount of exhaust CO, CO2 and HC under different engine speeds of 1500, 2500, 3500 and 4500.

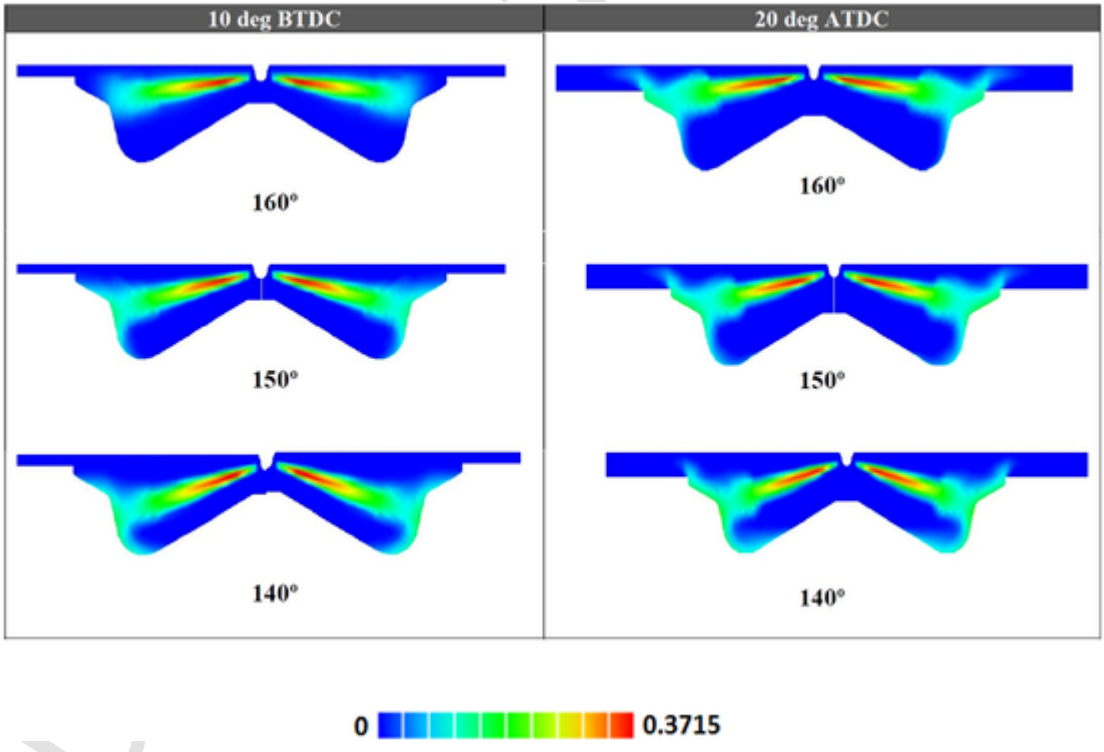

Fig. 10. Schematic of fuel distribution for different spray angles at 10 and 20 crank angles After Top Dead Center (ATDC).

0.0042 to 0.009 m, the swirl ratio and TKE for the three considered fuels were increased by 10 % and 4%, respectively, at around 5° BTDC. A higher swirl ratio (especially before fuel injection) caused by modifying the combustion chamber geometry or injection angle in a CI engine can improve combustion efficiency and increase fuel consumption. The bowl center depth of Tm3 caused more TKE, as shown in Fig. 14, which has beneficial effects on air-fuel mixing and leads to reduced ignition delay.

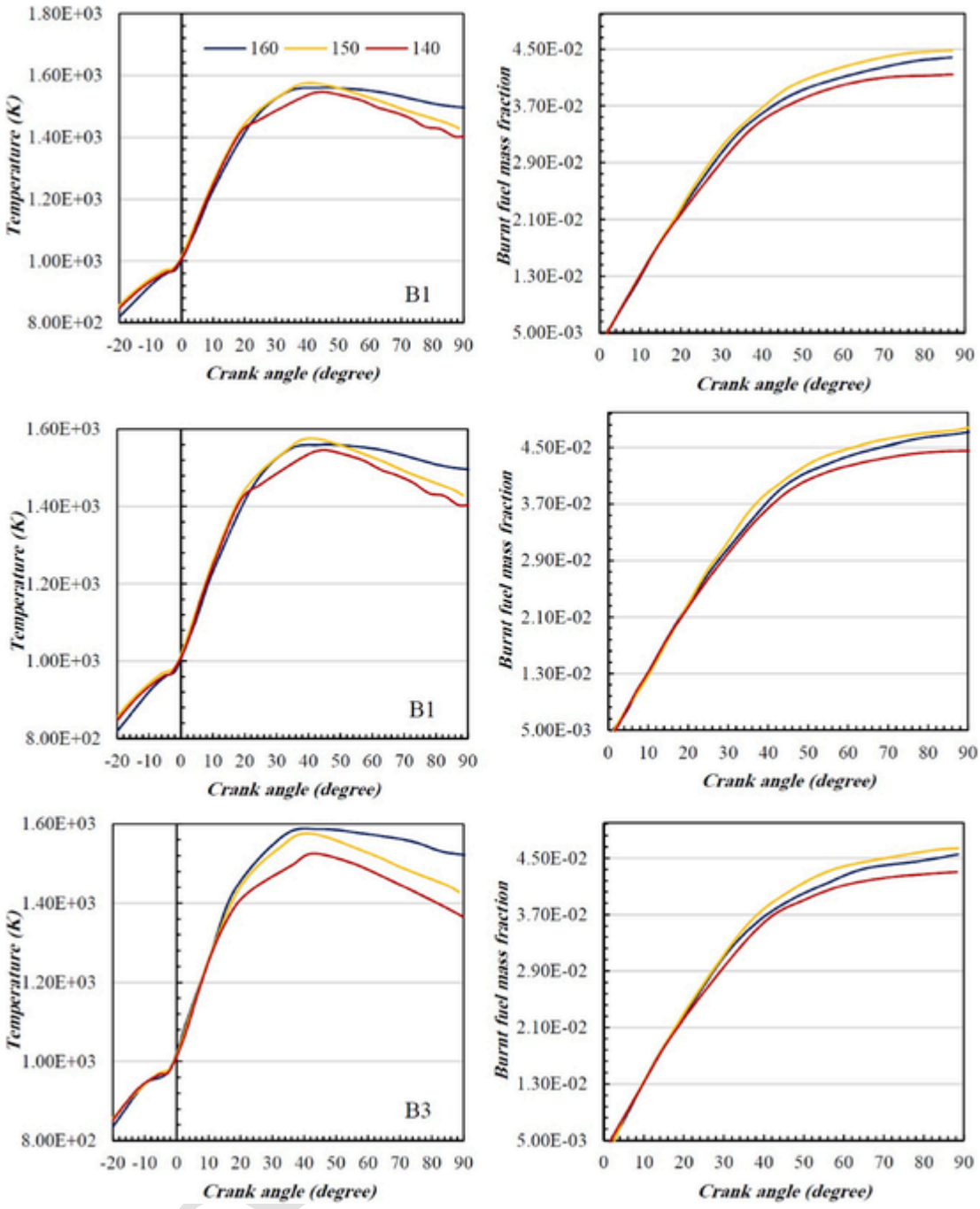

Fig. 11. Cylinder temperature and burnt fuel mass fraction at 2500 rpm for different biodiesels.

As seen in Fig. 15, the thermal efficiency for B3 was not changed by modifying the piston bowl geometry, but for the B1 and B2 fuels, changing Tm1 from 0.0042 to 0.007 or 0.009 m led to increased thermal efficiency by 3.44 %. As observed in Figs. 14 and 15, Tm3 created more swirl ratio compared with other BCDs, and the main reason for the higher NO and indicated power of Tm3 for the three considered fuels was the better air-fuel mixing caused by Tm3, which led to complete combustion, higher indicated power, and NO emissions (higher in-cylinder temperature). However, the soot oxidation of Tm3 was lower than that of the other BCDs due to the increasing temperature (caused by increasing swirl).

The compression ratio is known as a method for enhancing the emission and combustion characteristics of a diesel engine (Reddy et al., 2015). Compression ratios of 16, 20, and 24 were considered and varied by changing the piston bowl geometries for fuels B1, B2, and B3 under different engine speeds and full load conditions. The effects of the compression ratio on BSFC for different biodiesels are shown in Fig. 16. As can be seen, BSFC was significantly reduced by the increase in compression ratio from 16 to 24, which could be explained by the improved combustion processes and less heat losses at the same load and engine speed. BSFC diminished due to the improved efficiency of the thermodynamic cycle in the first place. It was observed that at a higher compression ratio, B3 had a higher BSFC compared to other fuels. It was also found that BSFC was reduced by around 20 % when the compression ratio was increased from 16 to 24 for B1, B2, and B3 (Almost the same results for other engine speeds have been obtained, but the results are presented for 2500 rpm). As observed, B2 had lower

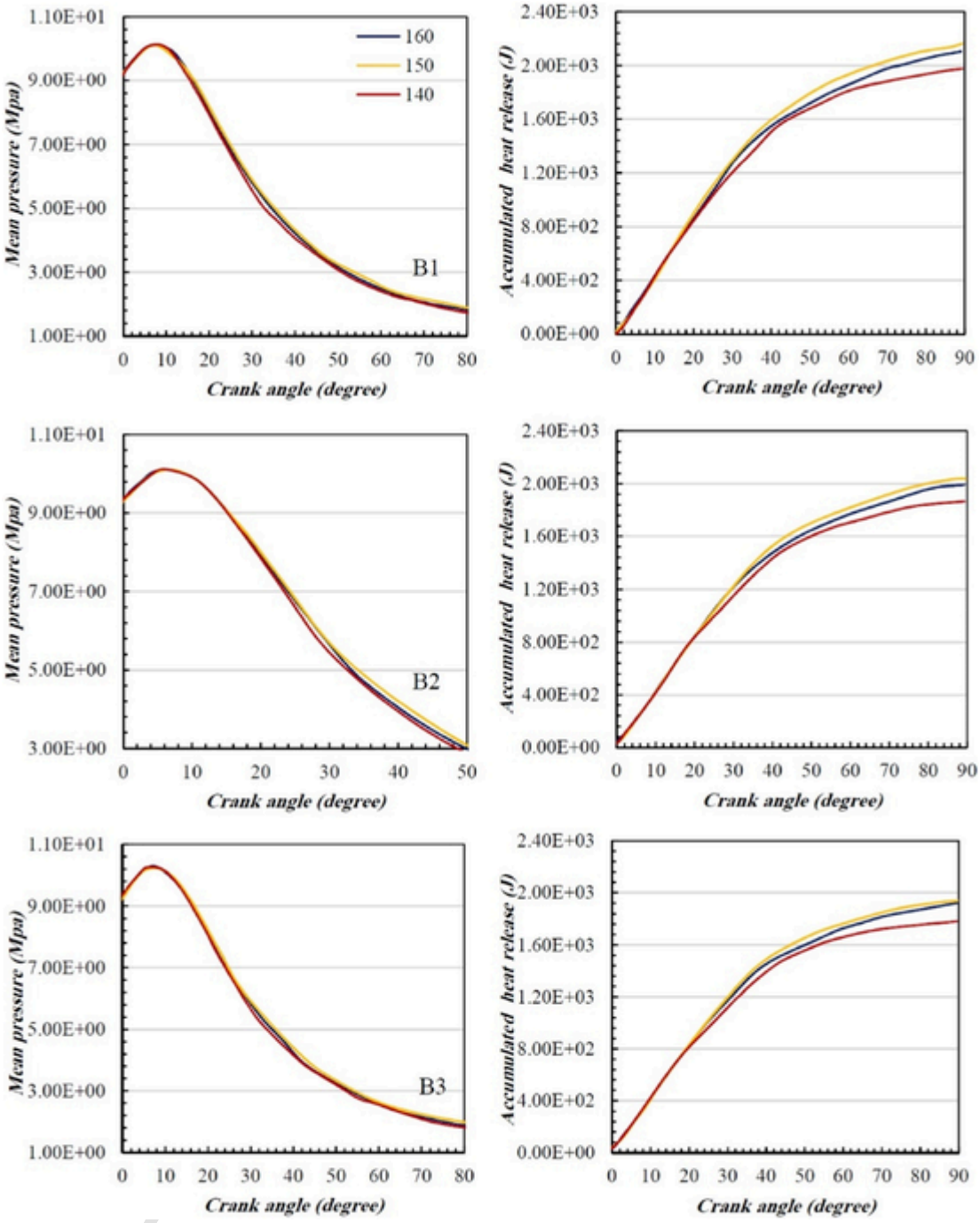

Fig. 12. Cylinder pressure and accumulated heat release at 2500 rpm for different biodiesels.

BSFC compared to B3 due to its lower viscosity and better air-fuel mixing, so injected fuel could be consumed more than B3. Actually, the higher viscosity of B3 led to increased spray particle size and combustion delay, causing incomplete combustion (Woo and Kim, 2019). In the compression ratio of 24, the viscosity of B3 was reduced by the higher temperature of the cylinder, and the undesirable effects of high viscosity on combustion characteristics can be imperceptible. It should be noted that the in-cylinder temperature of the engine fueled by B3 was not enough to resolve the undesirable effects of high viscosity on the engine performance in the compression ratio of 20.

Peak cylinder pressure generation is an essential factor in investigating the combustion process of the engine. Cylinder pressure at compression ratios of 16, 20, and 24 were calculated and investigated under the engine speed of 2500 rpm and can be seen in Fig. 17. As illustrated, the peak pressure was around 15.4 Mpa for all considered fuels at a compression ratio of 24 and was reduced by around 40 % when the compression ratio was decreased to 16. As can be seen, B2 and B1 have higher peak pressure at all compression ratios, which can be justified by the fact that B3 has a higher viscosity, which may explain the lower peak pressure of this fuel compared to B1 and B2 at these compression ratios, as also mentioned in reference EL_Kassaby and Nemit_allah (2013a). Common biodiesels have low volatility and higher viscosity which give a poor performance under lower compression ratios. Therefore, higher compression ratios are suggested for all considered biodiesels so as to obtain a better in-cylinder temperature and pressure, which will resulting in appropriate droplet atomization and

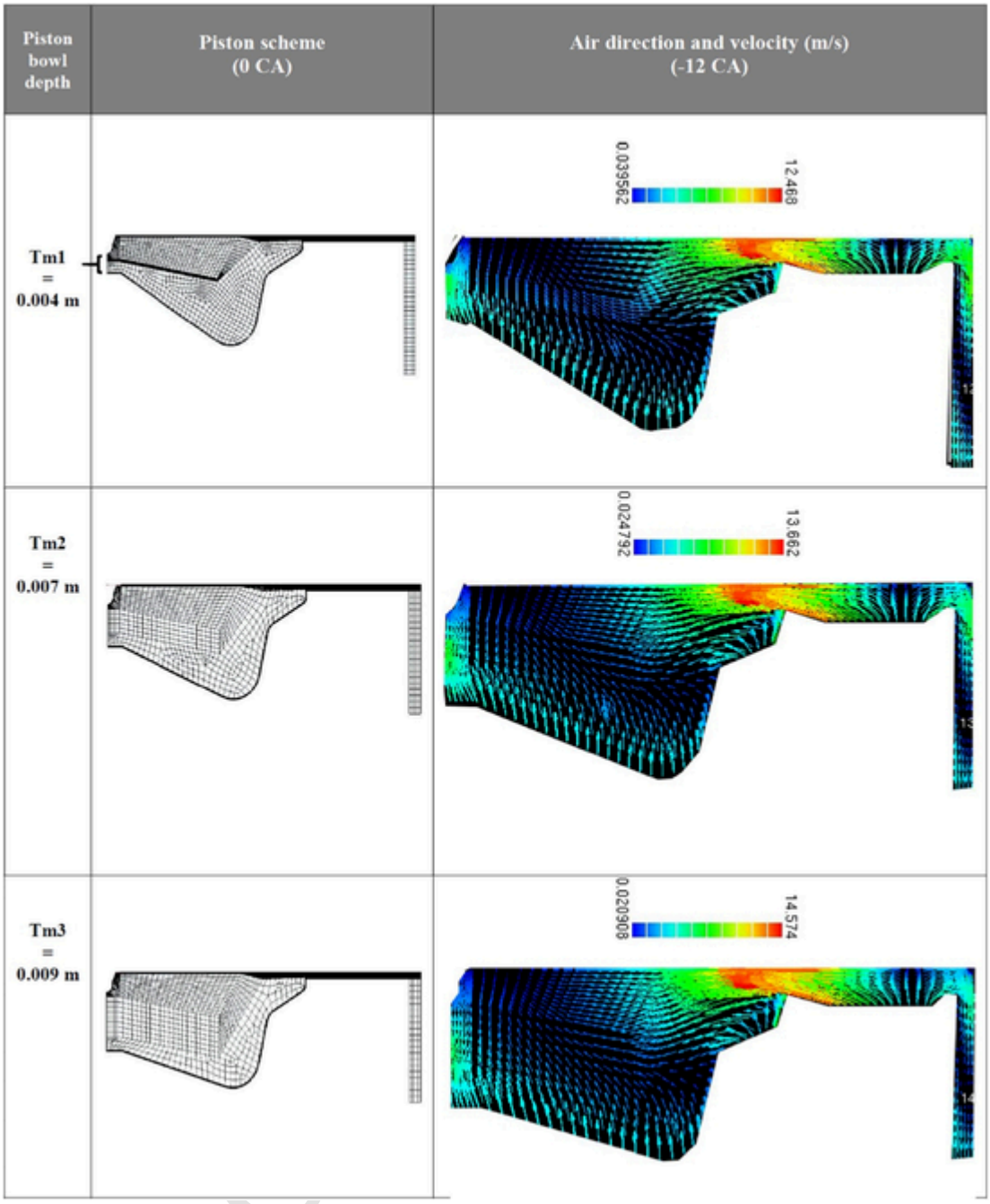

Fig. 13. Air direction and velocity for three piston bowl center depth (Tm) lengths considered before fuel injection.

combustion. In high temperatures, the lower BSFC of B3 is due to the existing enhanced amount of oxygen in B3 that led to improved combustion compared with B1 and B2 (EL_Kassaby and Nemit_allah, 2013b).

As illustrated in Fig. 18, the engine torque for all considered fuels decreased as the compression ratio decreased, and using B3 led to a reduction in the engine torque. As an example, a compression ratio of 16 using B2 increased the engine torque compared to B3 by around 1%, because B3 has higher viscosity, so it operates worse than B2. It should be noted that a biodiesel with high viscosity will perform better at higher compression ratios because of increasing in-cylinder pressure and temperature, which leads to good droplet atomization and combustion. Therefore, a higher compression ratio is suggested for B3 (EL_Kassaby and Nemit_allah, 2013a).

As seen in Fig. 15, the thermal efficiency for B3 was not changed by modifying the piston bowl geometry; for fuels B1 and B2, however, changing Tm1 from 0.0042 to 0.007 or 0.009 m increased thermal efficiency by 3.44 %. As can be seen in Figs. 14 and 15, Tm3 created more swirl ratio compared to other BCDs, and the main reason for the higher NO and indicated power of Tm3 for the three considered fuels was better air-fuel mixing caused by Tm3, which led to complete combustion, higher indicated power, and NO emission (higher in-cylinder temperature). However, soot oxidation was lower for Tm3 than for other BCDs due to the increasing temperature (caused by increasing swirl).

The NO emissions against fuel at different compression ratios for the various considered fuels are compared in Fig. 19. As can be seen in the figure, B2 produced higher NO emissions than B3 at all compres-

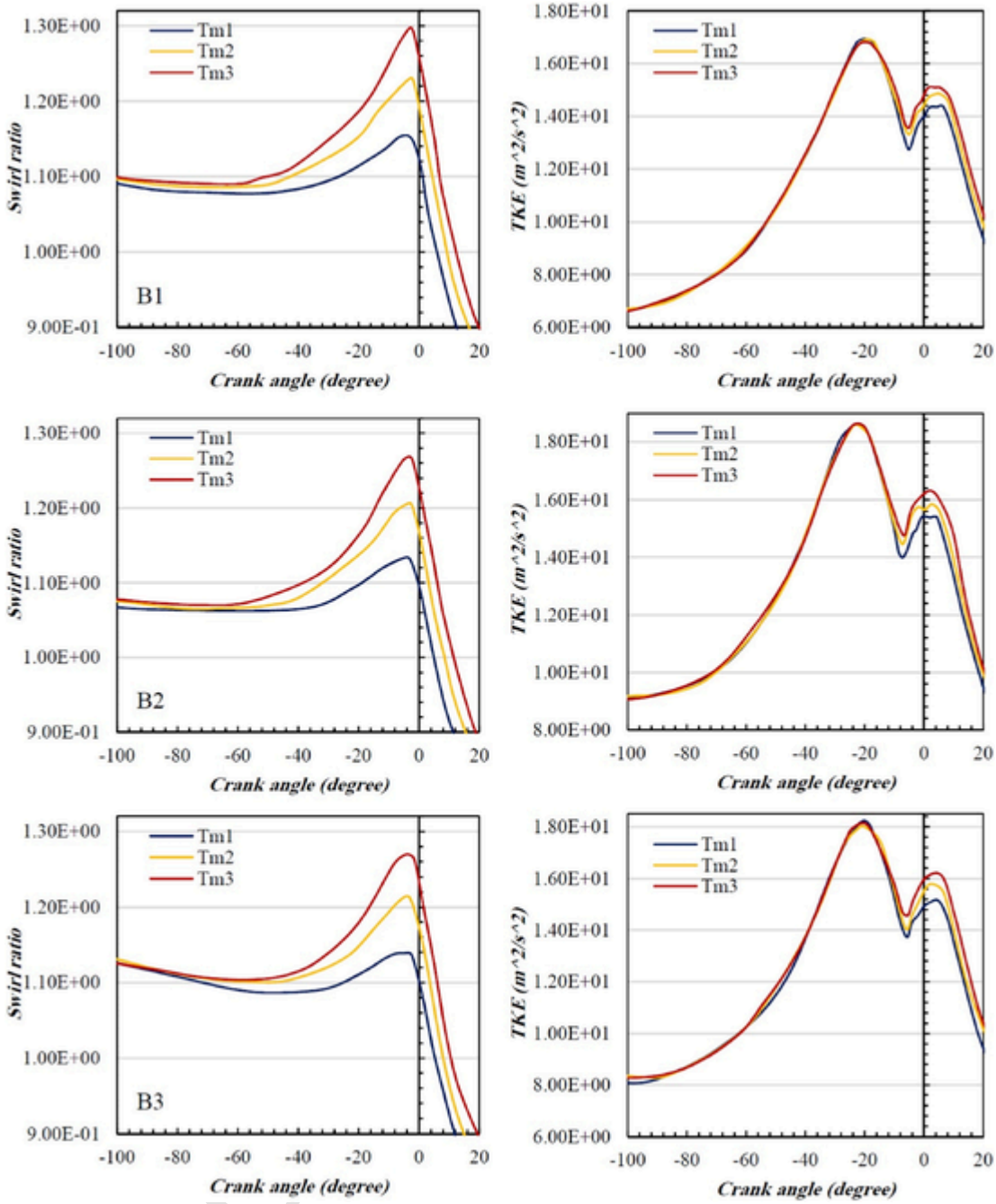

Fig. 14. Swirl ratio and TKE distributions at different crank angles for fuels of B1, B2, and B3 under 2500 rpm engine speed.

sion ratios. For B2, the exhaust NO remains higher than for B3 and B1 at compression ratios of 16 and 20. These can be justified by the fact that B2 has lower viscosity compared to B3 and also has a higher calorific value compared to B1, which leads to more complete combustion and higher in-cylinder temperatures at compression ratios of 16 and 20. However, the engine fueled by B1 produced higher NO emissions at the compression ratio of 24 compared to the other compression ratios.

3.4. Comparing two different FAMEs with pure diesel

In this section, the equivalence ratio for pure diesel and two FAMEs are investigated under an engine speed of 3500 rpm. As shown in Fig. 20, the equivalence ratio (ER) distributions for the engine fueled by B2 as a low viscosity biodiesel and B3 as a high viscosity biodiesel were compared with that of the engine fueled by pure diesel. Lower equivalence ratios are seen for B2 at EVO (exhaust valve closing) compared with B3 and diesel, which implies enhanced air-fuel mixing. It was determined that the higher oxygen content of B2 led to a lower mean equivalence ratio compared with pure diesel, and the lower viscosity of B2 explains its better ER compared with B3.

4. Conclusion

The present work investigated the effects of operational conditions, piston bowl geometry, and injection angle on the combustion and emission characteristics of a CI engine fueled by different vegetable biodiesels. These fuels had different properties (carbon atoms, O—H bond, and viscosity). It was found that at compression ratios of 16 and

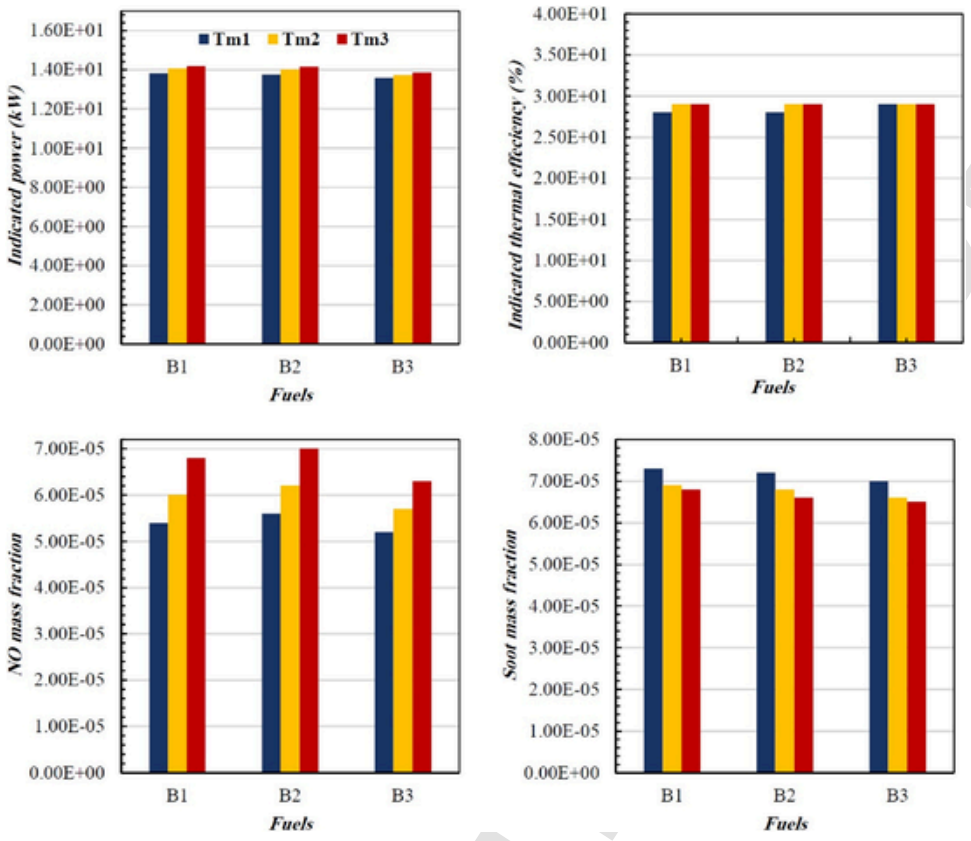

Fig. 15. Indicated thermal efficiency, power, NO and soot emissions for B1, B2, and B3 fuels.

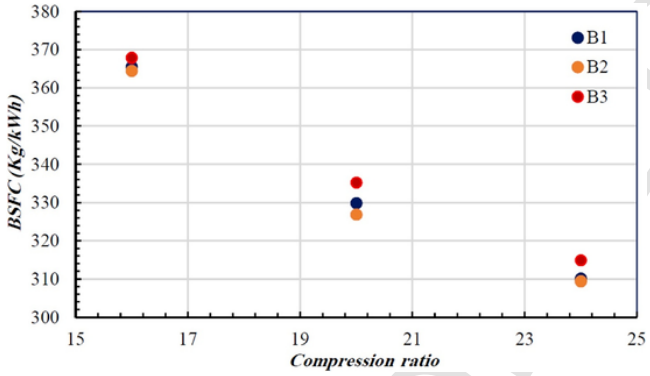

Fig. 16. Variation of BSFC at different compression ratios for fuels of B1, B2 and B3 under 2500 rpm engine speed.

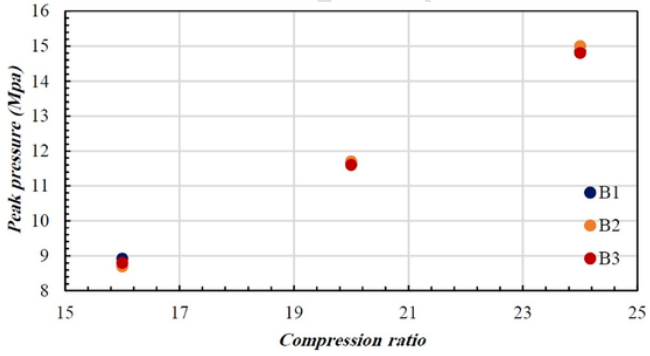

Fig. 17. Variation of peak pressure at different compression ratios for fuels of B1, B2 and B3 under 2500 rpm engine speed.

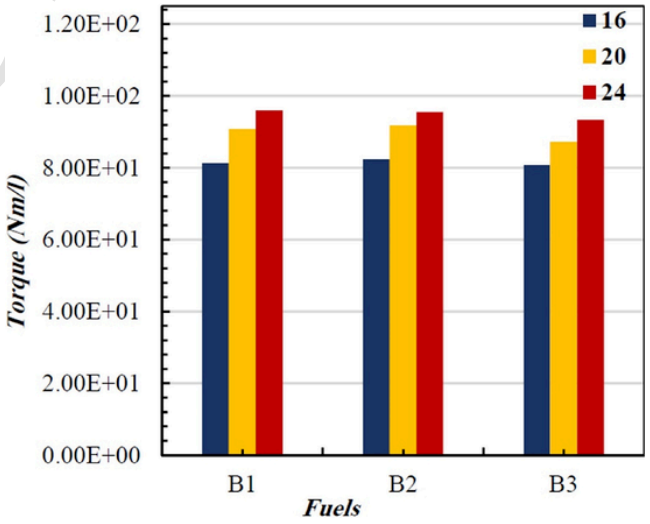

Fig. 18. Torque at different compression ratios for B1, B2, and B3 fuels under 2500 rpm engine speed.

24, all considered biodiesels had almost identical BSFC values. However, in a compression ratio of 20, B3 had higher BSFC compared with B1 and B2, showing that high and low compression ratios do not have identical effects on the engine fueled by each biodiesel. Here, B3 had higher BSFC in a compression ratio of 20 due to its higher viscosity compared with B2 and B1. Particularly, in this compression ratio, the in-cylinder temperature of the engine fueled by B3 was not enough to resolve the undesirable effect of high viscosity on engine performance. Therefore, the degree of difference in the viscosity value between the two biodiesels should be considered. In addition, air-fuel mixing in B3 is poor, and it caused a higher ER distribution compared with B2 and

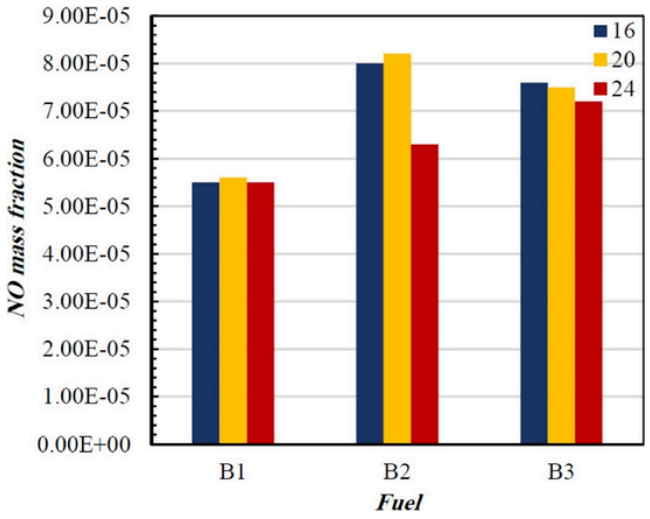

Fig. 19. Exhaust NO emissions at different compression ratios for B1, B2, and B3 fuels under 2500 rpm engine speed.

pure diesel in the engine. The results also showed that the higher oxygen content in B2 along with the equal number of carbon atoms compared with diesel fuel explain its lower ER compared with pure diesel. For future research, the effects of using different biodiesels with different viscosity values should be more exactly examined under different compression ratios in other different types of internal combustion engines, like heavy duty diesel engines.

Declaration of Competing Interest

None.

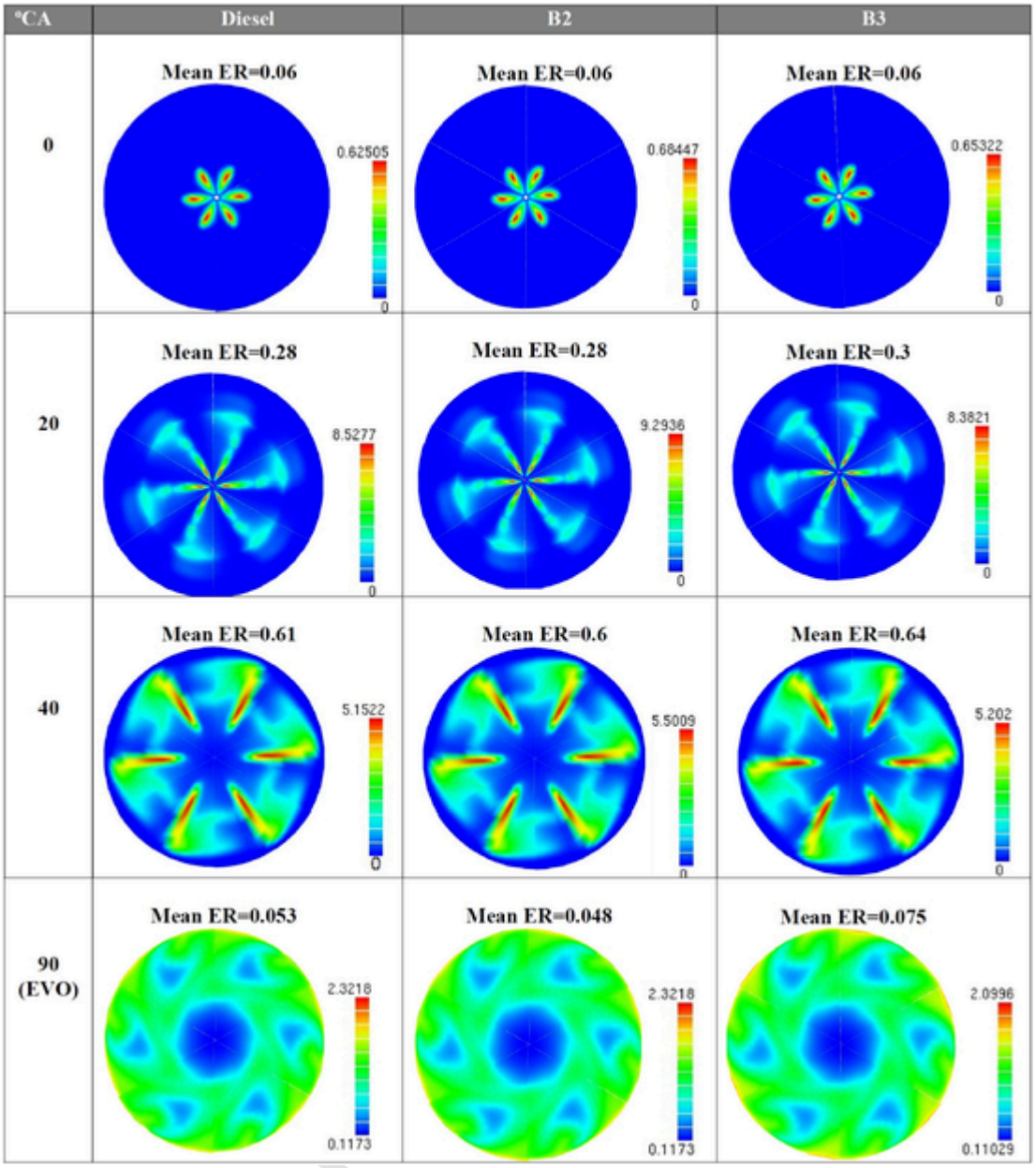

Fig. 20. Comparison of in-cylinder ER distribution at 0, 20, 40 and 90 CAs for B2, B3, and diesel.

References

Ramadhas, A., Muraleedharan, C., Jayaraj, S., 2005. Performance and emission evaluation of a diesel engine fueled with methyl esters of rubber seed oil. Renew. Energy 30 (12), 1789–1800.

Jiaqiang, E., et al., 2016a. Effects of fatty acid methyl esters proportion on combustion and emission characteristics of a biodiesel fueled diesel engine. Energy Convers. Manage. 117, 410–419.

Abu-Jrai, A., et al., 2009. Performance, combustion and emissions of a diesel engine operated with reformed EGR. Comparison of diesel and GTL fuelling. Fuel 88 (6), 1031–1041.

Xu, M., et al., 2016. Effect of diesel pre-injection timing on combustion and emission characteristics of compression ignited natural gas engine. Energy Convers. Manage. 117, 86–94.

Roy, M.M., 2009. Effect of fuel injection timing and injection pressure on combustion and odorous emissions in DI diesel engines. J. Energy Resour. Technol. 131 (3).

Raeie, N., Emami, S., Sadaghiyani, O.K., 2014. Effects of injection timing, before and after top dead center on the propulsion and power in a diesel engine. Propuls. Power Res. 3 (2), 59–67.

Fang, T., et al., 2008. Effects of injection angles on combustion processes using multiple injection strategies in an HSDI diesel engine. Fuel 87 (15–16), 3232–3239.

Yadollahi, B., Boroomand, M., 2013. The effect of combustion chamber geometry on injection and mixture preparation in a CNG direct injection SI engine. Fuel 107, 52–62.

Jiaqiang, E., et al., 2016b. Effects of fatty acid methyl esters proportion on combustion and emission characteristics of a biodiesel fueled diesel engine. Energy Convers. Manage. 117, 410–419.

Choi, S., et al., 2015. The effects of the combustion chamber geometry and a double-row nozzle on the diesel engine emissions. J. Automob. Eng. 229 (5), 590–598.

Li, J., et al., 2014. Effects of piston bowl geometry on combustion and emission characteristics of biodiesel fueled diesel engines. Fuel 120, 66–73.

Lee, S., Jeon, J., Park, S., 2016. Optimization of combustion chamber geometry and operating conditions for compression ignition engine fueled with pre-blended gasoline-diesel fuel. Energy Convers. Manage. 126, 638–648.

Yaliwal, V., et al., 2016. Effect of nozzle and combustion chamber geometry on the performance of a diesel engine operated on dual fuel mode using renewable fuels. Renew. Energy 93, 483–501.

EL_Kassaby, M., Nemit_allah, M.A., 2013a. Studying the effect of compression ratio on an engine fueled with waste oil produced biodiesel/diesel fuel. Alexandria Eng. J. 52 (1), 1–11.

Kakaee, A.-H., et al., 2016. Effects of piston bowl geometry on combustion and emissions characteristics of a natural gas/diesel RCCI engine. Appl. Therm. Eng. 102, 1462–1472.
Buyukkaya, E., 2010. Effects of biodiesel on a DI diesel engine performance, emission and combustion characteristics. Fuel 89 (10), 3099–3105.
Dubey, P., Gupta, R., 2017. Effects of dual bio-fuel (Jatropha biodiesel and turpentine oil) on a single cylinder naturally aspirated diesel engine without EGR. Appl. Therm. Eng. 115, 1137–1147.
Ibrahim, A., 2016. Performance and combustion characteristics of a diesel engine fuelled by butanol–biodiesel–diesel blends. Appl. Therm. Eng. 103, 651–659.
Yang, P.-M., et al., 2016. Emission evaluation of a diesel engine generator operating with a proportion of isobutanol as a fuel additive in biodiesel blends. Appl. Therm. Eng. 100, 628–635.
Mobasheri, R., Peng, Z., 2013. CFD investigation of the effects of re-entrant combustion chamber geometry in a HSDI diesel engine. Int. Scholarly Sci. Res. Innov. 7 (4), 770–780.
Kapusta, Ł.J., Teodorczyk, A., 2012. Numerical simulations of a simultaneous direct injection of a liquid and gaseous fuel into constant volume chamber. J. Power Technol. 92 (1), 12–19.
Mobasheri, R., Peng, Z., 2012. A Computational Investigation Into the Effects of Included Spray Angle on Heavy-duty Diesel Engine Operating Parameters. SAE Technical Paper.
Manual, A.A.F.U., C. Fire, Solver, 2013. Version.
Semenov, I., et al., 2013. Mathematical models and numerical algorithm for the dynamics of gasdroplets flows investigations using high performance computing. In: International Conference on Parallel and Distributed Computing Systems.
Pizza, G., et al., 2007. Evaporating and non-evaporating diesel spray simulation: comparison between the ETAB and wave breakup model. Int. J. Veh. Des. 45 (1–2), 80–99.
Shahbazi, M.R., et al., 2012. Biodiesel production via alkali-catalyzed transesterification of Malaysian RBD palm oil–characterization, kinetics model. J. Taiwan Inst. Chem. Eng. 43 (4), 504–510.
Singh, S., Singh, D., 2010. Biodiesel production through the use of different sources and characterization of oils and their esters as the substitute of diesel: a review. Renewable Sustainable Energy Rev. 14 (1), 200–216.
Özgür, C., Tosun, E., 2017. Prediction of density and kinematic viscosity of biodiesel by artificial neural networks. Energy Sour. Part A Recov. Util. Environ. Eff. 39 (10), 985–991.
Li, J., et al., 2017. Soot and NO emissions control in a natural gas/diesel fuelled RCCI engine by φ-T map analysis. Combust. Theory Model. 21 (2), 309–328.
Yang, W., et al., 2015a. Impact of urea direct injection on NOx emission formation of diesel engines fueled by biodiesel. In: ASME 2015 Internal Combustion Engine Division Fall Technical Conference. American Society of Mechanical Engineers Digital Collection.
Yang, Z., et al., 2015b. Effects of H2 addition on combustion and exhaust emissions in a diesel engine. Fuel 139, 190–197.
Li, J., Yang, W., Zhou, D., 2016. Modeling study on the effect of piston bowl geometries in a gasoline/biodiesel fueled RCCI engine at high speed. Energy Convers. Manage. 112, 359–368.
Kakaee, A.-H., Rahnama, P., Paykani, A., 2015. Influence of fuel composition on combustion and emissions characteristics of natural gas/diesel RCCI engine. J. Nat. Gas Sci. Eng. 25, 58–65.
Chen, Z., et al., 2014. Combustion and emissions characteristics of high n-butanol/diesel ratio blend in a heavy-duty diesel engine and EGR impact. Energy Convers. Manage. 78, 787–795.
Kalligeros, S., et al., 2003. An investigation of using biodiesel/marine diesel blends on the performance of a stationary diesel engine. Biomass Bioenergy 24 (2), 141–149.
Reşitoğlu, İ.A., Altinişik, K., Keskin, A., 2015. The pollutant emissions from diesel-engine vehicles and exhaust aftertreatment systems. Clean Technol. Environ. Policy 17 (1), 15–27.
Reddy, A., et al., 2015. Effect of compression ratio on the performance of diesel engine at different loads. Int. J. Eng. Res. Appl. 5 (10), 62–68.
Woo, D.G., Kim, T.H., 2019. Effect of kinematic viscosity variation with blended-oil biodiesel on engine performance and exhaust emission in a power tiller engine. Environ. Eng. Res. 25 (6), 946–959.
EL_Kassaby, M., Nemit_allah, M.A., 2013b. Studying the effect of compression ratio on an engine fueled with waste oil produced biodiesel/diesel fuel. Alexandria Eng. J. 52 (1), 1–11.